
This is an electronic reprint of the original article.
This reprint may differ from the original in pagination and typographic detail.

Ameziane, Maria; Mansell, Rhodri; Havu, Ville; Rinke, Patrick; van Dijken, Sebastiaan
Lithium-Ion Battery Technology for Voltage Control of Perpendicular Magnetization

Published in:
Advanced Functional Materials

DOI:
[10.1002/adfm.202113118](https://doi.org/10.1002/adfm.202113118)

Published: 01/07/2022

Document Version
Publisher's PDF, also known as Version of record

Published under the following license:
CC BY

Please cite the original version:
Ameziane, M., Mansell, R., Havu, V., Rinke, P., & van Dijken, S. (2022). Lithium-Ion Battery Technology for Voltage Control of Perpendicular Magnetization. *Advanced Functional Materials*, 32(29), Article 2113118. <https://doi.org/10.1002/adfm.202113118>

This material is protected by copyright and other intellectual property rights, and duplication or sale of all or part of any of the repository collections is not permitted, except that material may be duplicated by you for your research use or educational purposes in electronic or print form. You must obtain permission for any other use. Electronic or print copies may not be offered, whether for sale or otherwise to anyone who is not an authorised user.

Lithium-Ion Battery Technology for Voltage Control of Perpendicular Magnetization

Maria Ameziane, Rhodri Mansell, Ville Havu, Patrick Rinke, and Sebastiaan van Dijken*

The voltage control of magnetism is a promising path to the development of low-power spintronic devices. Magneto-ionics—exploiting voltage-driven ion migration to control magnetism—has attracted interest because it can generate large magnetoelectric effects at low voltage. Here, the use of the solid-state lithium-ion battery technology for reversible voltage-controlled switching between perpendicular and in-plane magnetization states in a Co–Pt bilayer is demonstrated. Due to the small size and high mobility of lithium ions, small voltages produce an exceptionally high magnetoelectric coupling efficiency of at least $7700 \text{ fJ V}^{-1} \text{ m}^{-1}$ at room temperature. The magnetic switching effect is attributed to the modulation of spin-orbit coupling at the Co–Pt interface when lithium ions migrate between a lithium storage layer (LiCoO_2) and the magnetic interface across a lithium phosphorous oxynitride (LiPON) solid-state electrolyte, which is corroborated by density functional theory calculations. Voltage control of magnetism in the battery structure does not show degradation over more than 500 voltage cycles, demonstrating promise for solid-state lithium-based magneto-ionic devices.

investigated,^[4–6] which can achieve faster charging, longer lifetimes, and higher energy densities.

Deterministic control of magnetic properties via voltage gating enables the design of low-power spintronic devices, including nonvolatile memory and logic,^[7–9] by minimizing the energy losses caused by Joule heating. Voltage control of magnetism via ion migration, or magneto-ionics, has emerged as a promising approach because the magnetic response to small voltages can be very strong compared to that of other magnetoelectric coupling mechanisms based on strain, exchange coupling, or charge carrier modulation.^[10,11] Magneto-ionics utilizing oxygen or hydrogen ions has been shown to alter the magnetic anisotropy,^[12–17] exchange bias,^[18,19,20] saturation magnetization,^[12–17,21–23] Curie temperature,^[21] Dzyaloshinskii–Moriya interaction (DMI),^[24] ferrimagnetic

order,^[25] and ferromagnetic resonance.^[26] The use of lithium ions has also attracted interest because of their small size, the capacity for reversible intercalation, and fast diffusion kinetics. Most studies have focused on the intercalation and deintercalation of lithium ions in spinel ferrite films using liquid electrolytes^[27–31] or solid-state heterostructures,^[32,33] demonstrating large changes of magnetization through bulk electrochemical processes. Moreover, metallic magnetic films have been manipulated through lithium insertion into amorphous CoFeB ^[34] or an adjacent antiferromagnetic oxide layer.^[35]


Many magnetic and spintronic devices, including magnetic hard disk drives,^[36] magnetic random-access memory (MRAM),^[37] magnetic racetrack memory,^[38] and proposals for magnetic logic,^[39] neuromorphic computing,^[40] and skyrmion-based devices^[41] utilize ultrathin ferromagnetic films with perpendicular magnetization. These technologies rely on magnetic switching, driven magnetization oscillations, or the motion of magnetic domain walls or skyrmions, induced by a magnetic field or electric current. In all applications, the saturation magnetization of the film does not change during device operation. For the development of low power spintronics, voltage control of magnetic switching without a reduction of magnetization is therefore crucial. This goal is particularly challenging for magneto-ionics, as electrochemical processes initiated by ion migration into or away from ultrathin ferromagnetic films tend to simultaneously alter the magnetic anisotropy and the saturation magnetization.^[12–17] Voltage-controlled switching between perpendicular and in-plane

1. Introduction

Lithium ions play a prominent role in modern rechargeable batteries for personal electronics and electric vehicles. Lithium-ion batteries combine high operating voltages with high-density energy storage into lightweight designs and operate efficiently under demanding conditions for many charging cycles.^[1–3] Most commercially available lithium-ion batteries rely on liquid electrolytes that often contain highly flammable organic substances that can constitute a hazard during use. To overcome this, all-solid-state architectures are being actively

M. Ameziane, R. Mansell, S. van Dijken
NanoSpin
Department of Applied Physics
Aalto University School of Science
P.O. Box 15100, Aalto FI-00076, Finland
E-mail: sebastiaan.van.dijken@aalto.fi

V. Havu, P. Rinke
Department of Applied Physics
Aalto University
Otakaari 1, Espoo FI-02150, Finland

 The ORCID identification number(s) for the author(s) of this article can be found under <https://doi.org/10.1002/adfm.202113118>.

© 2022 The Authors. Advanced Functional Materials published by Wiley-VCH GmbH. This is an open access article under the terms of the Creative Commons Attribution License, which permits use, distribution and reproduction in any medium, provided the original work is properly cited.

DOI: 10.1002/adfm.202113118

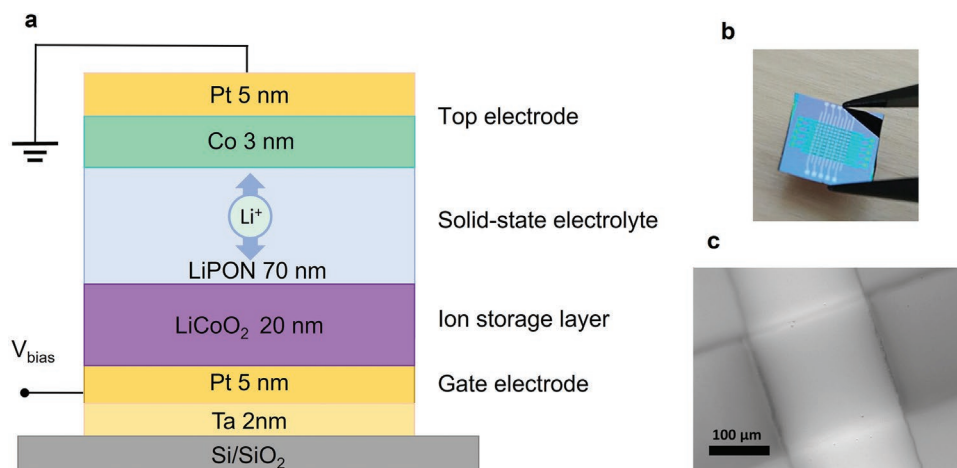


Figure 1. Magneto-ionic solid-state battery structure. a) Schematic of the multilayer stack and biasing configuration. b,c) Image of a $10 \times 10 \text{ mm}^2$ sample with multiple crossbar junctions and a close-up of a patterned battery structure.

magnetization states without loss of magnetization has been demonstrated in systems utilizing ionic-liquid gating^[42] or interface strain transfer.^[43]

Here, we demonstrate reversible voltage-controlled magnetic switching in a thin Co/Pt electrode layer using a solid-state lithium-ion battery structure. The magnetization of the Co film is switched from perpendicular to in-plane when lithium ions migrate from a LiCoO₂ storage layer into the Co/Pt electrode. The process, which operates at room temperature on a sub-second timescale, does not measurably alter the saturation magnetization of Co. Ab-initio calculations based on density functional theory (DFT) corroborate the experimental results. Our work demonstrates how the combination of miniaturized lithium-ion battery designs with relevant perpendicularly magnetized thin films can advance low-power spintronic devices.

2. Results

The magneto-ionic solid-state battery structure consists of a 2 nm Ta/5 nm Pt/20 nm LiCoO₂/70 nm LiPON/3 nm Co/5 nm Pt multilayer on top of a Si/SiO₂ substrate (Figure 1a). The entire stack is grown by magnetron sputtering at room temperature. In the battery structure, the LiCoO₂ film acts as a source of lithium ions^[44] (cathode) and the LiPON solid-state electrolyte efficiently transports the lithium ions between the LiCoO₂ storage layer and the Co/Pt electrode (anode).^[45,46] The multilayer is patterned into crossbar junctions (Figure 1b,c) with a junction size of $200 \times 200 \mu\text{m}^2$ using shadow-masking during film growth. Details of the fabrication process are given in the Experimental Section. During characterization, a bias voltage is applied to the Ta–Pt bottom electrode and the Co–Pt top electrode is grounded. Li⁺ ions thus migrate from the LiCoO₂ film through the LiPON electrolyte to the Co–Pt bilayer during the application of a positive voltage (discharge process). A negative voltage reverses the direction of Li⁺ ion migration (charge process). For all measurements the voltage is referenced to the power supply ground.

We first characterize the battery properties of the magneto-ionic junctions. Figure 2a shows cyclic voltammograms (CVs)

recorded at the start of and after extensive voltage cycling between -2.0 and $+2.5 \text{ V}$. The voltammograms display characteristics typical of a pseudocapacitive lithium-ion battery system, without sharp peaks that would indicate the presence of faradaic redox reactions.^[47,48] The changes observed in the CVs after cycling are likely due to local structural changes in the electrode layers induced by lithium insertion and de-insertion.^[49,50] We estimate the total charge storage capacity of the magneto-ionic battery cell by measuring galvanostatic charge–discharge curves under constant current flow (Figure 2b). The charge–discharge capacity (C) plotted in the graph is derived from $C = I\Delta t$, where I is the current and Δt is the charge–discharge time. The charge–discharge profiles are consistent also with those of a pseudocapacitive thin-film battery.^[47,48] The minor change in the charge–discharge behavior as a function of current, and thus the charging and discharging rate, indicate minimal capacity loss and a high degree of reversibility during voltage cycling.

A chronoamperometry measurement, shown in Figure 2c, was performed to evaluate the robustness of our magneto-ionic structure under repeated voltage switching. Here, the voltage was switched from -2 to $+2.5 \text{ V}$ in 2 s intervals for over 500 cycles, causing lithium ions to migrate to the Co/Pt electrode and back to the LiCoO₂ electrode, respectively. The measurement indicates a capacitor-like current decay after voltage switching with minor changes in the overall current profile after hundreds of cycles. The equilibrium current after voltage switching is reached in under 2 s . The minor decrease of peak currents over time is also believed to originate from structural changes to the system caused by lithium-ion migration into and out of electrode layers.^[49,50] The ionic conductivity of the LiPON layer was found to be $\approx 1.3 \times 10^{-6} \text{ S cm}^{-1}$ at room temperature and the activation energy for ion hopping was estimated as $0.34 \pm 0.02 \text{ eV}$ from electrochemical impedance spectroscopy measurements (Figure S1, Supporting Information). The ionic conductivity of the electrolyte is comparable to values reported in literature,^[51,52] while the activation energy is slightly lower than typically reported.^[51] These results combined show that the magneto-ionic crossbar junctions operate as stable, cyclable batteries with excellent lithium-ion transport properties.

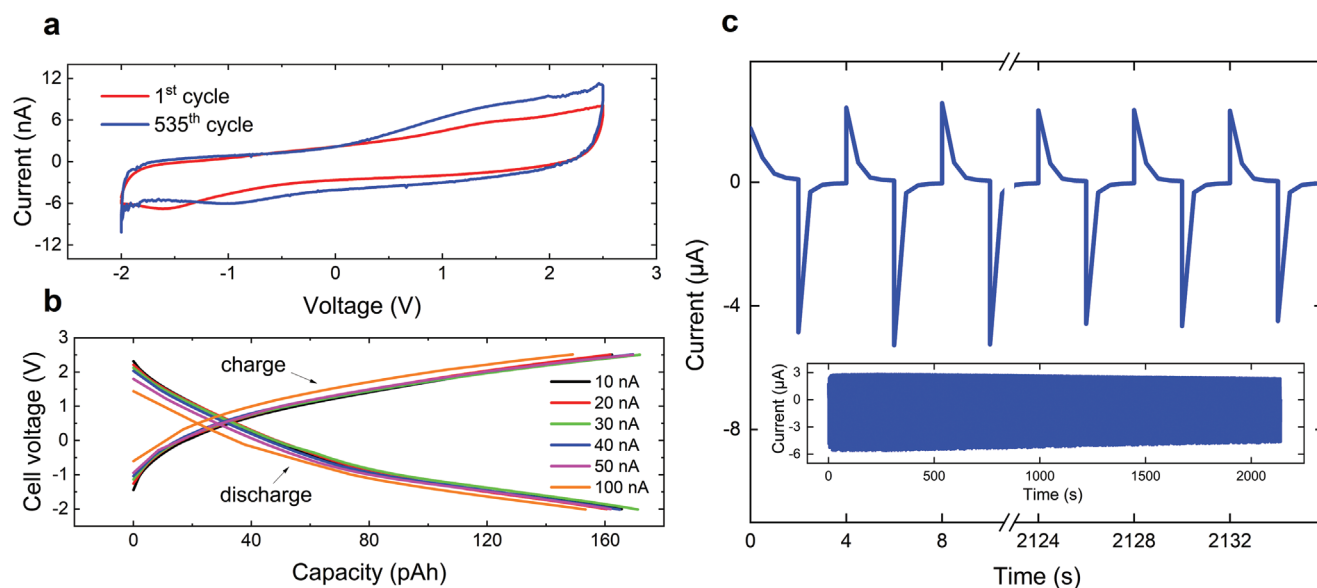


Figure 2. Electrical and electrochemical properties of the magneto-ionic battery. a) Cyclic voltammograms from -2.0 to $+2.5$ V recorded with a scan rate of 50 mV s^{-1} . Data obtained during the first and 535th cycle are shown. b) Charge–discharge capacity measured for constant current values. The charging curves were obtained under positive currents ranging from 10 to 100 nA with the discharge curves obtained under negative currents of the same magnitude. c) Chronoamperometry measurement performed by cycling the voltage between $+2.5$ and -2.0 V for over 500 times in 2 s intervals. The first and last three cycles of the measurement are displayed in the main graph.

Having demonstrated the battery behavior of the crossbar junctions, we move on to study the effects of an applied voltage on the magnetic layer. In **Figure 3a,b**, we show the voltage control of magnetic anisotropy through magneto-optical Kerr effect (MOKE) measurements. At -2.0 V, a square hysteresis curve with full remanence is recorded in a perpendicular magnetic field (**Figure 3a**), but no signal is measured for an in-plane magnetic field (**Figure 3b**). The effect is reversed at $+2.5$ V. Lithium-ion migration to the Co/Pt electrode under positive voltage thus switches the magnetization from

perpendicular to in-plane, while the removal of lithium from the Co/Pt bilayer at negative voltage restores the perpendicular magnetic anisotropy.

Figure 4 shows the voltage dependence of the polar MOKE loops in 0.5 V steps. Starting at -2.0 V in **Figure 4a**, the shape of the hysteresis curve transforms gradually with increasing voltage. At first, the hysteresis curve remains square on going from -2.0 to 0 V, while the coercivity decreases, consistent with an effect that alters the magnetic anisotropy but not the saturation magnetization. At $+1.0$ V, the magnetization switches

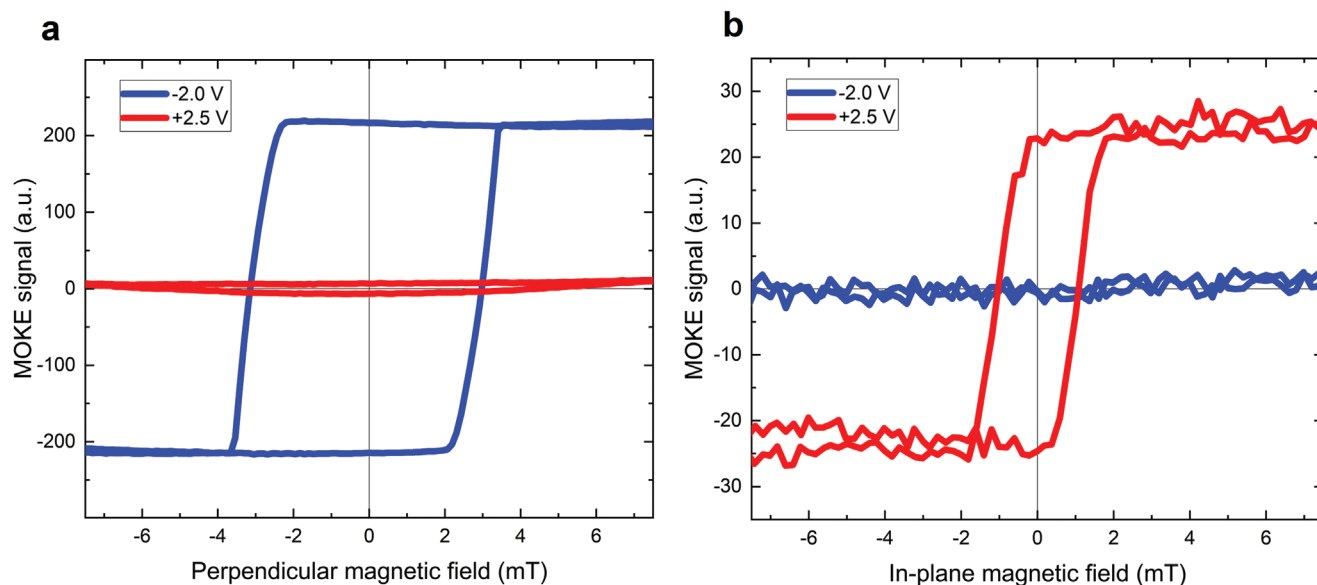


Figure 3. Voltage-driven magnetic switching between perpendicular and in-plane magnetization states. a) Polar MOKE hysteresis curves. b) Longitudinal MOKE hysteresis curves. The blue and red curves in (a) and (b) are recorded at -2.0 and $+2.5$ V, respectively.

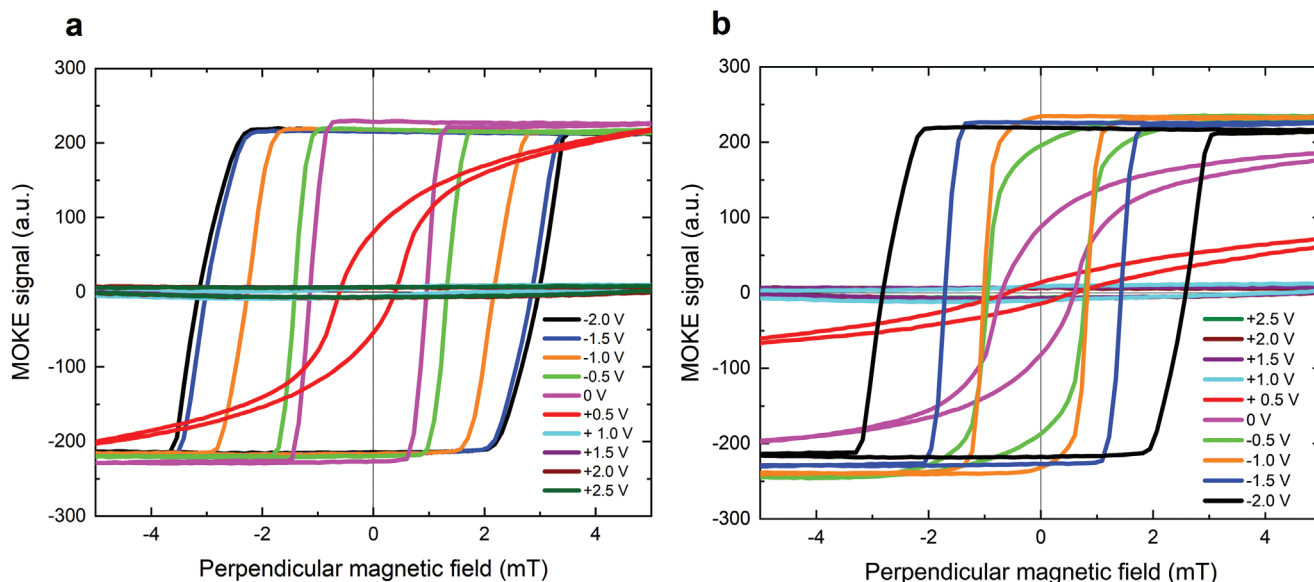


Figure 4. Voltage-control of magnetic anisotropy. a,b) Polar MOKE hysteresis curves recorded in the -2.0 to $+2.5$ V voltage range using 0.5 V intervals. The data for increasing and decreasing voltage shown in (a) and (b), respectively, correspond to lithium-ions migrating towards and away from the Co/Pt bilayer. The voltage dependence of longitudinal MOKE hysteresis curves is shown in Figure S2 (Supporting Information).

into the film plane and remains so as the voltage is stepped up to $+2.5$ V. Changing the voltage in the opposite direction by starting from $+2.5$ V has no visible effect until a $+0.5$ V gate voltage is reached (Figure 4b). Between $+0.5$ and -1.0 V, an increase in remanent magnetization is observed while the coercivity changes minimally. At -1.0 V, the magnetization is saturated perpendicular to the film at low applied fields and further decreasing the voltage gradually increases the coercivity. The increase of coercivity at increasingly negative voltages suggests that lithium ions continue to be extracted from the Co layer. There is also a hysteresis of the order of ≈ 0.5 V between the forward and backward voltage stepping directions, likely due to the activation energy for lithium-ion transport through the LiPON electrolyte that creates a potential barrier for ion migration. Figure S2 (Supporting Information) shows the voltage dependence of the longitudinal MOKE hysteresis curves. Interestingly, these curves do not show a significant variation of the in-plane saturation magnetization at positive voltages ranging from $+1.0$ to $+2.5$ V, i.e., when lithium ions are inserted effectively into the Co–Pt bilayer. These data complement the polar MOKE results of Figure 4 showing negligible changes in the saturation magnetization between -2.0 and 0 V. Insertion and de-insertion of lithium ions into Co/Pt therefore tunes the magnetic anisotropy from perpendicular to in-plane and vice versa without appreciably altering the saturation magnetization.

Repeated switching of the magnetization direction in zero magnetic field by voltage cycling between -2.0 and $+2.5$ V is demonstrated in Figure 5a,b. In these measurements, the perpendicular and in-plane magnetization components are defined as the ratio of remnant magnetization M_r and saturation magnetization M_s obtained from the polar and longitudinal MOKE hysteresis curves. The time scale of ion-induced magnetic switching is illustrated in Figure 5c. Changing the voltage from -2.0 to $+2.5$ V fully switches the magnetization from perpendicular to

in-plane within 2 s. Reversing the voltage back to -2.0 V abruptly decreases the longitudinal MOKE signal before a slower decay sets in. The timescale of magnetic switching corresponds to that of the chronoamperometry measurement shown in Figure 2c, signifying reversible migration of lithium ions as the origin of the effect. We attribute the asymmetry in the voltage-induced magnetic response to the large open-circuit voltage of the crossbar junction (-1.3 V). In solid-state batteries, asymmetry in the electrochemical potential is always present because of different electrodes (Co/Pt and LiCoO₂ in our battery structure). The magnitude of asymmetry in the ion-induced magnetic response is tailored by magnetic parameters such as the Co layer thickness. While magnetic saturation requires seconds at room temperature, most of the Co film magnetization reorients on a sub-second timescale. Reversible magnetic switching for 0.5 s voltage pulses is demonstrated in Figure S3 (Supporting Information) and a MOKE microscopy video of the experiment is provided as Video S1 (Supporting Information).

3. Discussion

The results shown in this paper demonstrate the potential of solid-state lithium-ion battery design principles for the development of novel functional magneto-ionic devices. Perpendicular magnetization in a Co–Pt bilayer originates from the interfacial spin-orbit interaction at the Co/Pt interface.^[53,54] The data in Figures 3–5 indicate that lithium insertion into the Co/Pt bilayer reduces the perpendicular interface anisotropy. Clear battery-like behavior (Figure 2) as well as the very short charge screening length of Co (≈ 0.1 nm) rule out electrostatic charge modulation at the Co/Pt interface as the origin of the voltage-induced magnetic effect. To further exclude electrostatic charge modulation as the dominant effect, we monitored

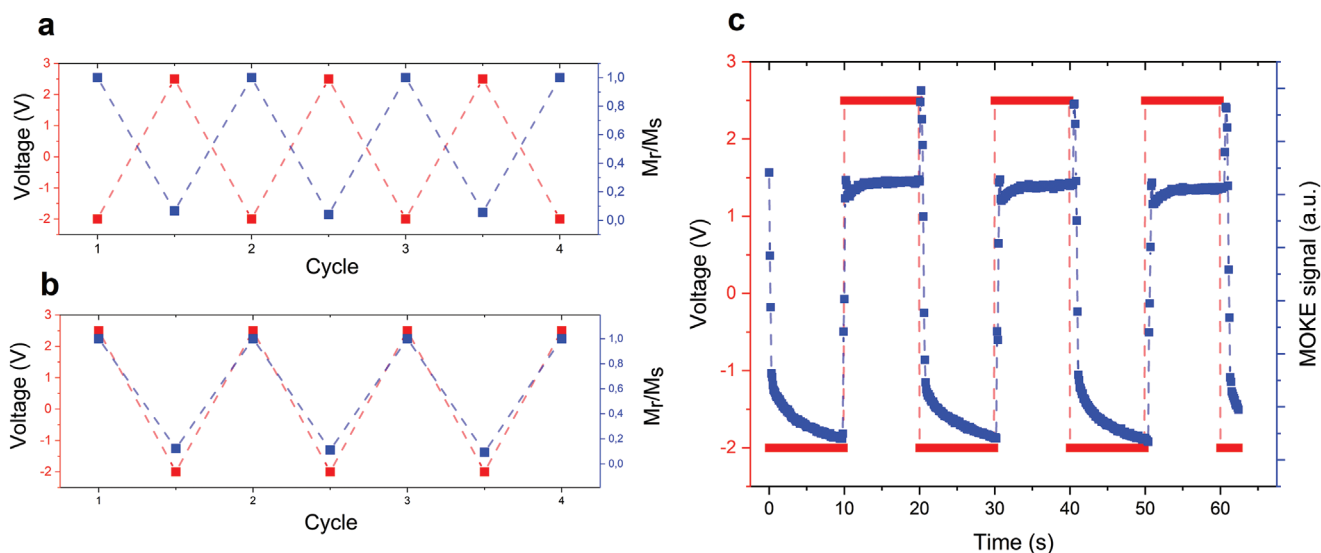


Figure 5. Reversibility and dynamics of voltage-controlled magnetic switching in a Ta/Pt/LiCoO₂/LiPON/Co/Pt battery structure. a,b) Reversible voltage-induced switching of a) the perpendicular magnetization and b) the in-plane magnetization in zero magnetic field. The data are derived from polar and longitudinal MOKE measurements after applying a voltage for 60 s. c) Time-resolved modulation of the longitudinal MOKE signal while toggling the voltage between −2.0 and +2.5 V in 10 s intervals. Figure S3 (Supporting Information) shows data for more than 60 switching cycles and a time interval of 0.5 s.

the magnetization configuration after turning the voltage off (Figure S4, Supporting Information). The experiments indicate nonvolatile magnetic behavior on a timescale of several minutes, in line with an ion-migration process.

To evaluate the magnetoelectric efficiency of our structure, we consider a magnetoelectric coupling coefficient $\alpha_{\text{ME}} = \Delta K_i / \Delta E$, where ΔK_i is the change in interfacial magnetic anisotropy energy between perpendicular and in-plane magnetization states and ΔE is the electric field across the solid electrolyte. From our data, the magnetoelectric coupling efficiency is estimated to be $\geq 7700 \text{ fJ V}^{-1} \text{ m}^{-1}$ (see Supporting Information), which is the strongest magnetoelectric effect reported to date. The performance of our device structure is promising in terms of energy efficiency, room-temperature operation, and its ability to switch the magnetization by small voltages while upholding the saturation magnetization. The latter property, which contrasts with other studies on magneto-ionic anisotropy control in thin ferromagnetic films,^[12–17] is likely due to the absence of redox processes in our lithium-based system. The lack of clear redox peaks in the CV data of Figure 2a suggests that magnetic switching proceeds via an intercalation/deintercalation process instead, whereby lithium intercalation modulates the hybridization of electron orbitals at the Co/Pt interface and, thus, K_i and deintercalation restores the perpendicular magnetic anisotropy. The effect of lithium on the magnetization and magnetic anisotropy of the Co film are corroborated by DFT calculations (Figure 6). Assuming a random distribution of lithium inside Co, we find that the average magnetic moment of Co only decreases by $\approx 12\%$ upon the insertion of 50% lithium (Figure 6a). In contrast, the magnetocrystalline anisotropy energy changes drastically, favoring perpendicular magnetization at low lithium concentration and in-plane magnetization above 40% lithium (Figure 6b). To estimate the number of migrating lithium ions in our experiments, we utilize the galvanostatic charge–discharge

curves in Figure 2b. At +2.5 V bias voltage, the estimated number of lithium ions migrating toward the Co layer is $\approx 3.7 \times 10^{12}$, which gives an upper limit of 34% lithium in the Co film in saturation (see Supporting Information). The experiments and DFT calculations thus provide the same qualitative picture: When lithium migrates into the Co layer upon the application of positive voltage pulses, the magnetization reorients from perpendicular to in-plane while the saturation magnetization of the Co film is mostly preserved.

4. Conclusion

We have demonstrated reversible voltage-controlled switching of the magnetization direction from perpendicular to in-plane at room temperature in a battery-inspired lithium-based magneto-ionic structure. The capacity to strongly modulate the magnetic anisotropy using modest voltages while preserving the saturation moment of a thin ferromagnetic film paves the way toward energy-efficient electric-field control of magnetism, which is relevant to a variety of applications in the fields of spintronics and neuromorphic computing. Further optimization to the structure's operation can be achieved by scaling down the device size and improving the structural and electronic properties of the solid-state electrolyte.

5. Experimental Section

Sample Fabrication: The magneto-ionic multilayer stack was grown by magnetron sputtering in a system with a base pressure of 3.0×10^{-8} mbar. The crossbars junctions were fabricated in two steps, with the layers deposited through metal shadow masks placed onto a $10 \times 10 \text{ mm}^2$ silicon substrate with 500 nm thermal oxide. First, the bottom electrode consisting of 2 nm Ta/5 nm Pt/20 nm LiCoO₂ was grown through a mask

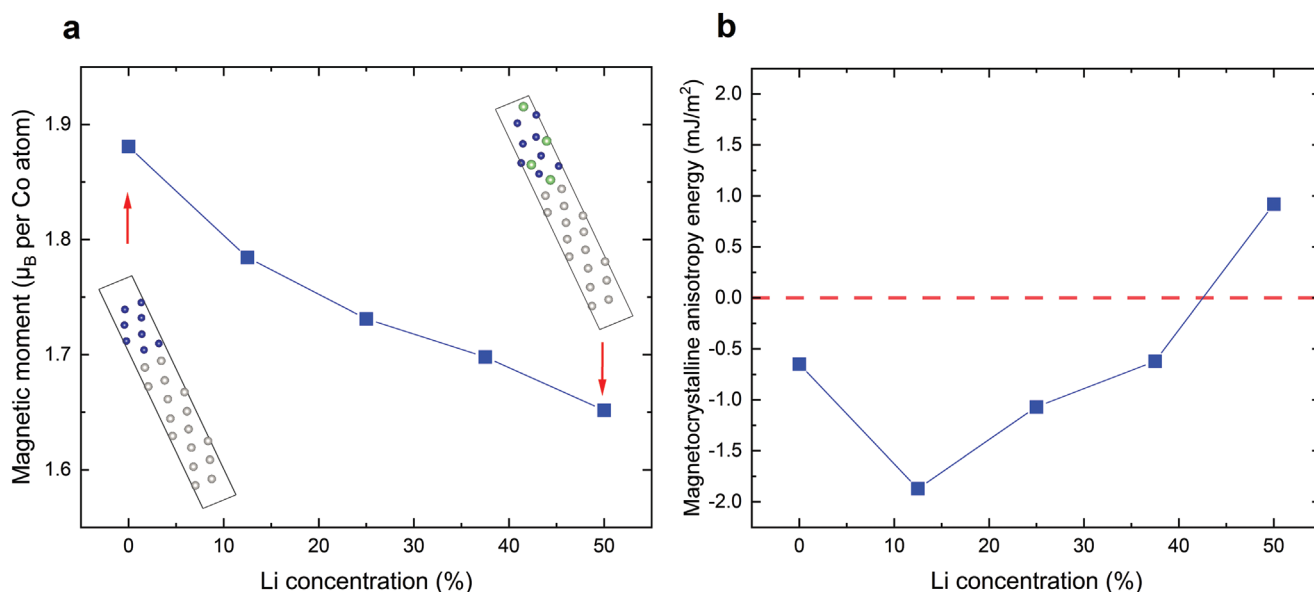


Figure 6. a) Calculated average magnetic moment per Co atom and b) magnetocrystalline anisotropy energy as a function of the lithium concentration in the Co film of a Co(111)/Pt(111) bilayer. The schematics in (a) illustrate the unit cells used in DFT calculations of a lithium-free Co layer (bottom left) and Co layer with 50% lithium (top right). In (b), negative (positive) values indicate that the magnetocrystalline anisotropy energy favors perpendicular (in-plane) magnetization.

with 200 μm -wide stripes. Ta and Pt were DC-sputtered in 30 sccm Ar flow and 60 sccm Ar flow, respectively. LiCoO_2 was RF-sputtered in 20 sccm Ar flow, which resulted in a nanocrystalline film (Figure S6, Supporting Information). In the second step, the mask is rotated by 90° and placed on top of the bottom electrode. The second half of the structure is then grown by first depositing a 70-nm-thick layer of LiPON in 20 sccm N_2 from a lithium phosphate (Li_3PO_4) target using RF sputtering. This step is followed by the growth of a 3 nm Co/5 nm Pt bilayer using DC sputtering to complete the structure. All layers were deposited at room temperature. Due to the high reactivity of as-grown LiPON films, the electrolyte layer was grown during the second half of the process to avoid exposure to atmosphere in between steps and to ensure good quality of the Co/LiPON interface. XPS measurements do not indicate significant oxidation of the Co film (Figure S7, Supporting Information).

Sample Characterization: The magnetic properties of the crossbar junctions were characterized using an Evico MOKE microscope equipped with two separate electromagnets to apply magnetic fields both perpendicular and parallel to the sample plane. For the application of voltages, the crossbars were electrically bonded using a 5330 F&S Bondtec wire-bonder. A Keithley 2450 source meter was added to the setup to simultaneously apply voltages during magnetic characterization and to perform electrical/electrochemical measurements, including cyclic voltammetry, chronoamperometry, and galvanostatic charge and discharge measurements. Electrochemical impedance spectroscopy data were collected using an E4980A Agilent Precision LCR meter.

DFT Calculations: First-principles calculations are a powerful tool to assess the effects of atom migration on the magnetic moment and anisotropy of thin ferromagnetic films.^[55] DFT calculations were performed using the projector augmented-wave (PAW) method with a Perdew–Burke–Ernzerhof (PBE) exchange–correlation functional implemented in VASP.^[56–61] The calculation geometry was constructed by relaxing bulk Co and Pt cells and bringing their (111) surfaces into contact. The authors considered four atomic layers of Co and 8 atomic layers of Pt. The in-plane lattice constant of Pt was set to 3.967 Å, a value obtained from bulk relaxation, while the Co atoms could relax. As a first step, the lithium-free geometry was relaxed using a $24 \times 24 \times 2$ k-point grid without spin-orbit coupling (SOC) and with an energy cutoff of 500 eV. The geometry was considered converged when the maximum

force on the atoms was less than $0.005 \text{ eV } \text{\AA}^{-1}$. Structural relaxation resulted in a slightly tilted unit cell along the perpendicular direction and a significant enlargement of the in-plane lattice constants of Co. The authors repeated this process for geometries with different lithium concentrations, with the lithium atoms being randomly distributed in the Co film. Two sets of self-consistent noncollinear calculations (SOC switched on) were carried out using a $12 \times 12 \times 1$ k-point grid; one with the magnetization aligned perpendicular to the Co film and one with in-plane magnetization. The magnetic anisotropy energy per unit area was calculated as the total energy difference between these two magnetization configurations.

Supporting Information

Supporting Information is available from the Wiley Online Library or from the author.

Acknowledgements

This work was supported by the Academy of Finland (Grant Nos. 316857 and 295269). The authors wish to acknowledge CSC – IT Center for Science, Finland, and the Aalto Science-IT project for computational resources.

Conflict of Interest

The authors declare no conflict of interest.

Data Availability Statement

The data that support the findings of this study are available from the corresponding author upon reasonable request.

Keywords

lithium-ion batteries, magnetic anisotropy, magnetic switching, magneto-ionics, voltage control of magnetism

Received: December 22, 2021

Revised: March 26, 2022

Published online: April 22, 2022

- [1] A. Manthiram, *ACS Cent. Sci.* **2017**, 3, 1063.
- [2] T. Kim, W. Song, *J. Mater. Chem. A* **2019**, 7, 2942.
- [3] A. Manthiram, *Nat. Commun.* **2020**, 11, 1550.
- [4] A. Mauger, C. M. Julien, A. Paoletta, M. Armand, K. Zaghib, *Materials* **2019**, 12, 3892.
- [5] Q. Zhao, S. Stalin, C. Z. Zhao, L. A. Archer, *Nat. Rev. Mater.* **2020**, 5, 229.
- [6] F. Wu, J. Maier, Y. Yu, *Chem. Soc. Rev.* **2020**, 49, 1569.
- [7] X. Li, A. Lee, S. A. Razavi, H. Wu, K. L. Wang, *MRS Bull.* **2018**, 43, 970.
- [8] J.-M. Hu, C.-W. Nan, *APL Mater.* **2019**, 7, 080905.
- [9] S. Manipatruni, D. E. Nikonov, C.-C. Lin, T. A. Gosavi, H. Liu, B. Prasad, Y.-L. Huang, E. Bonturim, R. Ramesh, I. A. Young, *Nature* **2019**, 565, 35.
- [10] C. Song, B. Cui, F. Li, X. Zhou, F. Pan, *Progr. Mater. Sci.* **2017**, 87, 33.
- [11] A. Molinari, H. Hahn, R. Kruk, *Adv. Mater.* **2019**, 31, 1806662.
- [12] C. Bi, Y. Liu, T. Newhouse-Illige, M. Xu, M. Rosales, J. W. Freeland, O. Mryasov, S. Zhang, S. G. E. T. Velthuis, W. G. Wang, *Phys. Rev. Lett.* **2014**, 113, 267202.
- [13] U. Bauer, L. Yao, A. J. Tan, P. Agrawal, S. Emori, H. L. Tuller, S. van Dijken, G. S. D. Beach, *Nat. Mater.* **2015**, 14, 174.
- [14] H.-B. Li, N. Lu, Q. Zhang, Y. Wang, D. Feng, T. Chen, S. Yang, Z. Duan, Z. Li, Y. Shi, W. Wang, W.-H. Wang, K. Jin, H. Liu, J. Ma, L. Gu, C. Nan, P. Yu, *Nat. Commun.* **2017**, 8, 2156.
- [15] A. Quintana, J. Zhang, E. Isarain-Chávez, E. Menéndez, R. Cuadrado, R. Robles, M. Dolors Baró, M. Guerrero, S. Pané, B. J. Nelson, C. M. Müller, P. Ordejón, J. Nogués, E. Pellicer, J. Sort, *Adv. Funct. Mater.* **2017**, 27, 1701904.
- [16] A. J. Tan, M. Huang, C. O. Avci, F. Büttner, M. Mann, W. Hu, C. Mazzoli, S. Wilkins, H. L. Tuller, G. S. D. Beach, *Nat. Mater.* **2019**, 18, 35.
- [17] A. J. Tan, M. Huang, S. Sheffels, F. Büttner, S. Kim, A. H. Hunt, I. Waluyo, H. L. Tuller, G. S. D. Beach, *Phys. Rev. Mater.* **2019**, 3, 064408.
- [18] D. A. Gilbert, A. J. Grutter, E. Arenholz, K. Liu, B. J. Kirby, J. A. Borchers, B. B. Maranville, *Nat. Commun.* **2016**, 7, 11050.
- [19] J. Zehner, R. Huhnstock, S. Oswald, U. Wolff, I. Soldatov, A. Ehresmann, K. Nielsch, D. Holzinger, K. Leistner, *Adv. Electron. Mater.* **2019**, 5, 1900296.
- [20] J. Zehner, D. Wolf, M. U. Hasan, M. Huang, D. Bono, K. Nielsch, K. Leistner, G. S. D. Beach, *Phys. Rev. Mater.* **2021**, 5, L061401.
- [21] Y. N. Yan, X. J. Zhou, F. Li, B. Cui, Y. Y. Wang, G. Y. Wang, F. Pan, C. Song, *Appl. Phys. Lett.* **2015**, 107, 122407.
- [22] N. Lu, P. Zhang, Q. Zhang, R. Qiao, Q. He, H. B. Li, Y. Wang, J. Guo, D. Zhang, Z. Duan, Z. Li, M. Wang, S. Yang, M. Yan, E. Arenholz, S. Zhou, W. Yang, L. Gu, C.-W. Nan, J. Wu, Y. Tokura, P. Yu, *Nature* **2017**, 546, 124.
- [23] A. Quintana, E. Menéndez, M. O. Liedke, M. Butterling, A. Wagner, V. Sireus, P. Torruella, S. Estradé, F. Peiró, J. Dendooven, C. Detavernier, P. D. Murray, D. A. Gilbert, K. Liu, E. Pellicer, J. Nogués, J. Sort, *ACS Nano* **2018**, 12, 10291.
- [24] L. Herrera Diez, Y. T. Liu, D. A. Gilbert, M. Belmeguenai, J. Vogel, S. Pizzini, E. Martinez, A. Lamperti, J. B. Mohammedi, A. Laborieux, Y. Roussigné, A. J. Grutter, E. Arenholz, P. Quarterman, B. Maranville, S. Ono, M. Salah El Hadri, R. Tolley, E. E. Fullerton, L. Sanchez-Tejerina, A. Stashkevich, S. M. Chérif, A. D. Kent, D. Querilloz, J. Langer, B. Ocker, D. Ravelosona, *Phys. Rev. Applied* **2019**, 12, 034005.
- [25] M. Huang, M. U. Hasan, K. Klyukin, D. Zhang, D. Lyu, P. Gargiani, M. Valvidares, S. Sheffels, A. Churikova, F. Büttner, J. Zehner, L. Caretta, K.-Y. Lee, J. Chang, J.-P. Wang, K. Leistner, B. Yildiz, G. S. D. Beach, *Nat. Nanotechnol.* **2021**, 16, 981.
- [26] M. Guan, L. Wang, S. Zhao, Z. Zhou, G. Dong, W. Su, T. Min, J. Ma, Z. Hu, W. Ren, Z.-G. Ye, C.-W. Nan, M. Liu, *Adv. Mater.* **2018**, 30, 1802902.
- [27] S. Dasgupta, B. Das, M. Knapp, R. A. Brand, H. Ehrenberg, R. Kruk, H. Hahn, *Adv. Mater.* **2014**, 26, 4639.
- [28] T. Yamada, K. Morita, K. Kume, H. Yoshikawa, K. Awaga, *J. Mater. Chem. C* **2014**, 2, 5183.
- [29] X. Zhu, J. Zhou, L. Chen, S. Guo, G. Liu, R. W. Li, W. D. Lu, *Adv. Mater.* **2016**, 28, 7658.
- [30] Q. Zhang, X. Luo, L. Wang, L. Zhang, B. Khalid, J. Gong, H. Wu, *Nano Lett.* **2016**, 16, 583.
- [31] S. Dasgupta, B. Das, Q. Li, D. Wang, T. T. Baby, S. Indris, M. Knapp, H. Ehrenberg, K. Fink, R. Kruk, H. Hahn, *Adv. Funct. Mater.* **2016**, 26, 7507.
- [32] T. Tsuchiya, K. Terabe, M. Ochi, T. Higuchi, M. Osada, Y. Yamashita, S. Ueda, M. Aono, *ACS Nano* **2016**, 10, 1655.
- [33] G. Wei, L. Wei, D. Wang, Y. Chen, Y. Tian, S. Yan, L. Mei, J. Jiao, *Appl. Phys. Lett.* **2017**, 110, 062404.
- [34] D. Pravarthana, B. Wang, Z. Mustafa, S. Agarwal, K. Pei, H. Yang, R.-W. Li, *Phys. Rev. Applied* **2019**, 12, 054065.
- [35] Z. Mustafa, D. Pravarthana, B. Wang, H. Yang, R.-W. Li, *Phys. Rev. Applied* **2020**, 14, 014062.
- [36] S. N. Piramanayagam, *J. Appl. Phys.* **2007**, 102, 011301.
- [37] A. D. Kent, D. C. Worledge, *Nat. Nanotechnol.* **2015**, 10, 187.
- [38] S. Parkin, S.-H. Yang, *Nat. Nanotechnol.* **2015**, 10, 195.
- [39] Z. Luo, A. Hrabec, T. Phuong Dao, G. Sala, S. Finizio, J. Feng, S. Mayr, J. Raabe, P. Gambardella, L. J. Heyderman, *Nature* **2020**, 579, 214.
- [40] J. Grollier, D. Querilloz, K. Y. Camsari, K. Everschor-Sitte, S. Fukami, M. D. Stiles, *Nat. Electron.* **2020**, 3, 360.
- [41] A. Fert, N. Reyren, V. Cros, *Nat. Rev. Mater.* **2017**, 2, 17031.
- [42] S. Zhao, L. Wang, Z. Zhou, C. Li, G. Dong, L. Zhang, B. Peng, T. Min, Z. Hu, J. Ma, W. Ren, Z.-G. Ye, W. Chen, P. Yu, C.-W. Nan, M. Liu, *Adv. Mater.* **2018**, 30, 1801639.
- [43] Y. Shirahata, R. Shiina, D. López González, K. J. A. Franke, E. Wada, M. Itoh, N. A. Pertsev, S. van Dijken, T. Taniyama, *NPG Asia Mater.* **2015**, 7, e198.
- [44] K. Mizushima, P. C. Jones, P. J. Wiseman, J. B. Goodenough, *Mater. Res. Bull.* **1980**, 15, 783.
- [45] X. Yu, J. Bates, G. Jellison, F. Hart, *J. Electrochem. Soc.* **1997**, 144, 524.
- [46] Y. Y. Ren, K. Chen, R. J. Chen, T. Liu, Y. B. Zhang, C.-W. Nan, *J. Am. Ceram. Soc.* **2015**, 98, 3603.
- [47] V. Augustyn, P. Simon, B. Dunn, *Energy Environ. Sci.* **2014**, 7, 1597.
- [48] M. R. Lukatskaya, B. Dunn, Y. Gogotsi, *Nat. Commun.* **2016**, 7, 12647.
- [49] V. J. Ovejias, A. Cuadras, *Sci. Rep.* **2019**, 9, 14875.
- [50] J. P. Pender, G. Jha, D. H. Youn, J. M. Ziegler, I. Andoni, E. J. Choi, A. Heller, B. S. Dunn, P. S. Weiss, R. M. Penner, C. B. Mullins, *ACS Nano* **2020**, 14, 1243.
- [51] X. Yu, J. B. Bates, G. E. Jellison, F. X. Hart, *J. Electrochem. Soc.* **1997**, 144, 524.
- [52] S. Nowak, F. Berkemeier, G. Schmitz, *J. Power Sources* **2015**, 275, 144.
- [53] N. Nakajima, T. Koide, T. Shidara, H. Miyauchi, H. Fukutani, A. Fujimori, K. Iio, T. Katayama, M. Nývlt, Y. Suzuki, *Phys. Rev. Lett.* **1998**, 81, 5229.

- [54] F. Hellman, A. Hoffmann, Y. Tserkovnyak, G. S. D. Beach, E. E. Fullerton, C. Leighton, A. H. MacDonald, D. C. Ralph, D. A. Arena, H. A. Dürr, P. Fischer, J. Grollier, J. P. Heremans, T. Jungwirth, A. V. Kimel, B. Koopmans, I. N. Krivorotov, S. J. May, A. K. Petford-Long, J. M. Rondinelli, N. Samarth, I. K. Schuller, A. N. Slavin, M. D. Stiles, O. Tchernyshyov, A. Thiaville, B. L. Zink, *Rev. Mod. Phys.* **2017**, 89, 025006.
- [55] K. Klyukin, G. Beach, B. Yildiz, *Phys. Rev. Mater.* **2020**, 4, 104416.
- [56] G. Kresse, J. Hafner, *Phys. Rev. B* **1993**, 47, 558.
- [57] G. Kresse, J. Hafner, *Phys. Rev. B* **1994**, 49, 14251.
- [58] G. Kresse, J. Furthmüller, *Comput. Mat. Sci.* **1996**, 6, 15.
- [59] G. Kresse, J. Furthmüller, *Phys. Rev. B* **1996**, 54, 11169.
- [60] P. E. Blöchl, *Phys. Rev. B* **1994**, 50, 17953.
- [61] G. Kresse, D. Joubert, *Phys. Rev. B* **1999**, 59, 1758.